In Vivo Measurement of Local Aortic Pulse-Wave Velocity in Mice With MR Microscopy at 17.6 Tesla

Volker Herold,[1]* Marco Parczyk,[1] Philipp Mörchel,[1] Christian H. Ziener,[1] Gert Klug,[2] Wolfgang R. Bauer,[2] Eberhard Rommel,[1] and Peter M. Jakob[1]

Transgenic mouse models of human diseases have gained increasing importance in the pathophysiology of cardiovascular diseases (CVD). As an indirect measure of vascular stiffness, aortic pulse-wave velocity (PWV) is an important predictor of cardiovascular risk. This study presents an MRI approach that uses a flow area method to estimate local aortic pulse-wave velocity at different sites in the murine aorta. By simultaneously measuring the cross-sectional area and the through-plane velocity with a phase-contrast CINE method, it was possible to measure average values for the PWV in the ascending and descending aorta within the range of 2.4–4.3 m/s for C57BL/6J mice (ages 2 and 8 months) and apoE-knockout mice (age 8 months). Statistically significant differences of the mean values of the PWV of both groups could be determined. By repeating CINE measurements with a time delay of 1 ms between two subsequent data sets, an effective temporal resolution of 1000 frames/s (fps) could be achieved. Magn Reson Med 61: 1293–1299, 2009. © 2009 Wiley-Liss, Inc.

Key words: high-field MRI; trigger; pulse-wave velocity; QA-method; phase contrast; ApoE-KO; mouse aorta

Cardiovascular disease (CVD) still remains among the most common causes of death. Hemodynamic changes in the large and medium sized arteries caused by increased arterial stiffness are supposed to serve as early indications of CVD (1,2). Alterations in the aortic morphology and function occur with advancing age and result in changes of functional parameters such as aortic distensibility and pulse-wave velocity (3,4).

Pulse-wave velocity (PWV), which is known to increase with increasing arterial stiffness, has proven to be an independent predictor of cardiovascular risk and mortality in certain cases of CVD (2,5,6). Phenotypes of mice genetically deficient in apolipoprotein E (apoE-KO) spontaneously develop atherosclerosis at the arterial wall accompanied with the occurrence of a severe hyperlipidemia (7). Several studies provide evidence that human atherosclerotic lesions resemble to a certain degree those found in the murine arteries, and thus mark the apoE-KO mouse as an important model of human atherosclerosis (8,9).

[1]Julius-Maximilians-Universität Würzburg, Lehrstuhl für Experimentelle Physik 5, Würzburg, Germany.

[2]Julius-Maximilians-Universität Würzburg, Medizinische Universitätsklinik, Würzburg, Germany.

Grant sponsor: Deutsche Forschungsgemeinschaft; Grant number: SFB 688.

*Correspondence to: Volker Herold, Physikalisches Institut, EP 5, Universität Würzburg, Am Hubland, D-97074 Würzburg, Germany. E-mail: vrherold@physik.uni-wuerzburg.de

Received 2 April 2008; revised 12 December 2008; accepted 18 December 2008.

DOI 10.1002/mrm.21957

Published online 7 April 2009 in Wiley InterScience (www.interscience.wiley.com).

High field MRI has proven to be a suitable tool to monitor morphological and functional parameters of the cardiovascular system in mice (10,11). Changes of the arterial morphology during atherosclerotic plaque progression can be detected at various sites of the murine aorta (12–14). Several studies verified a high correlation between histopathological findings and the results of MR measurements at different stages of atherosclerotic diseases (15,16). Electrocardiogram-triggered and respiratory-gated MR has been able to quantify morphological parameters of atherosclerotic lesions (17). In particular MRI methods developed for the measurement of pulse-wave velocity and arterial compliance in humans (18–21) have not been accessible in mice due to the faster heartbeat and small size of the murine anatomy.

Doppler ultrasound-based transit-time (TT) methods have been applied to mice and have provided first results of an average PWV over the propagation pathway (22–24). The TT approach delivers a mean value of the PWV, which is a function of the vessel wall thickness, the vessel diameter and the local elastic modulus (25). Because lesions are scattered along the vessel wall in early stages of atherosclerosis, the real PWV is dependent on the location along the propagation pathway. To overcome the limitations of masking local elastic properties, Vulliémoz et al. proposed a MR-based method to measure local PWV by exploiting the flow area (QA) relation during early systole (26,27). Using noninvasive ultrasonic measurements, the QA method was applied to estimate local PWV in the murine carotid artery (28). By making functional vascular parameters accessible, ultrasonic methods have shown the ability to characterize cardiovascular functional phenotypes in mice, whereas MRI has to date only been used for the quantification of morphological parameters. MRI, however, offers a wide range of imaging possibilities that could also enhance the quality of investigating the cardiovascular function in mice.

In humans, MRI has already proven to be an all-embracing imaging method for the investigation of morphological and functional arterial system parameters (29,30). Recent studies provide several methodological approaches to monitor functional parameters such as arterial pulse-wave velocity in humans (18,19,21,27).

This study presents a method of imaging the local aortic PWV at different locations using high field MRI at 17.6T. By using a QA approach, magnetic resonance imaging was shown to be a versatile method allowing the assessment of morphological information at a high spatial resolution as well as estimations of local PWV at different locations in the murine aorta.

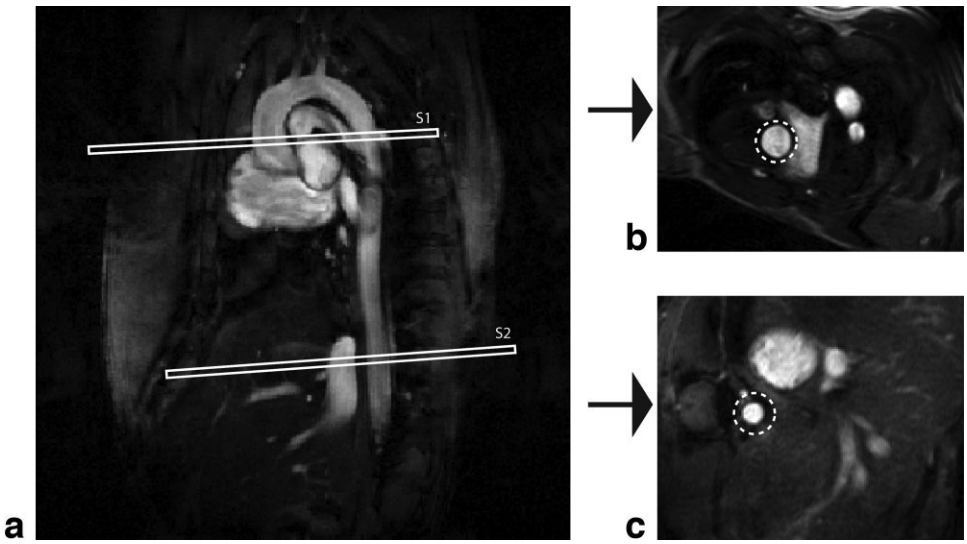

FIG. 1. **a:** Slice positioning for the local PWV measurements. **b:** Ascending aorta. **c:** Abdominal aorta.

METHODS

QA Method

The basic assumption for using the relation between the variation of flow and area measurements is that all relevant data is acquired during a wave reflection-free period of the cardiac cycle. The early systolic wave at certain locations of the human arterial system is known to be reflectionless (25). Previously published data on the local PWV in the carotid artery provide evidence that the same holds for the murine aorta (28). Assuming a unidirectional and reflection-free incident pulse wave, the characteristic impedance Z_c is equal to the ratio between pressure variation (dP) and flow variation (dQ):

$$Z_C = \frac{dP}{dQ} = \frac{dP}{dA}\frac{dA}{dQ} = \frac{1}{C_A}\frac{dA}{dQ}. \quad [1]$$

Where $C_A = dA/dP$ is the local area compliance of the vessel. The solution of the wave equation also suggests a relation between Z_c and C_A:

$$Z_C = \sqrt{\frac{\rho}{\overline{A}}\frac{1}{C_A}}. \quad [2]$$

ρ and $\overline{A}$ are the blood density and the time-averaged cross-sectional area of the vessel. PWV as a function of C_A is given by:

$$PWV = \sqrt{\frac{\overline{A}}{\rho}\frac{1}{C_A}}. \quad [3]$$

Multiplication of Equations [3] and [2] using [1] gives the PWV as a function of the variation of blood flow and cross-sectional area (27).

$$PWV = \frac{dQ}{dA}. \quad [4]$$

Animal Care

Local PWV was examined in five C57BL/6J mice at the age of 2 months and 8 months and nine 8 month old apoE-KO mice. The apoE-KO mice were fed with a high cholesterol diet (TD 88137, Harlan Winkelmann, The Netherlands) for a period of 10 weeks before the MR measurements. The mice were anesthetized during the MR experiments with an isoflurane inhalation (1.5–2.0 Vol.%) O_2 (2 L/min) applied by means of a nose cone. Due to the small inner diameter of the gradient insert and the radio frequency (RF) coil, the mouse temperature could be kept constant at 37°C during the MR measurements by adjusting the temperature of the gradient cooling unit. All experimental procedures were in accordance with institutional guidelines and were approved by local authorities.

MR Imaging

MR experiments were performed on a Bruker AVANCE 750 (Bruker Biospin, Rheinstetten, Germany) spectrometer with a vertical main magnetic field of 17.6 Tesla (T) and a bore size of 89 mm. The spectrometer was equipped with a self-shielded gradient insert with a maximum gradient strength of 1000 mT/m and an inner diameter of 40 mm. For RF transmission and detection, mice were placed vertically (head up) in a home built transverse electromagnetic (TEM) resonator with an inner diameter of 27 mm. Cardiac and respiratory trigger signals were detected using a pressure sensitive balloon. The pressure signal was transformed into an electrical signal outside the gradient coil and was post processed in real-time with a homebuilt amplification unit. Interferences with the rapidly switching strong gradient fields could thus be avoided.

To localize the ascending and descending aorta, the imaging protocol started with a set of two-dimensional (2D) FLASH experiments. For measuring the local PWV, two image slices were positioned perpendicular to the ascending aorta and the abdominal aorta as depicted in Fig. 1. To acquire flow and area information, a phase-contrast CINE method (PC CINE method) was applied. The

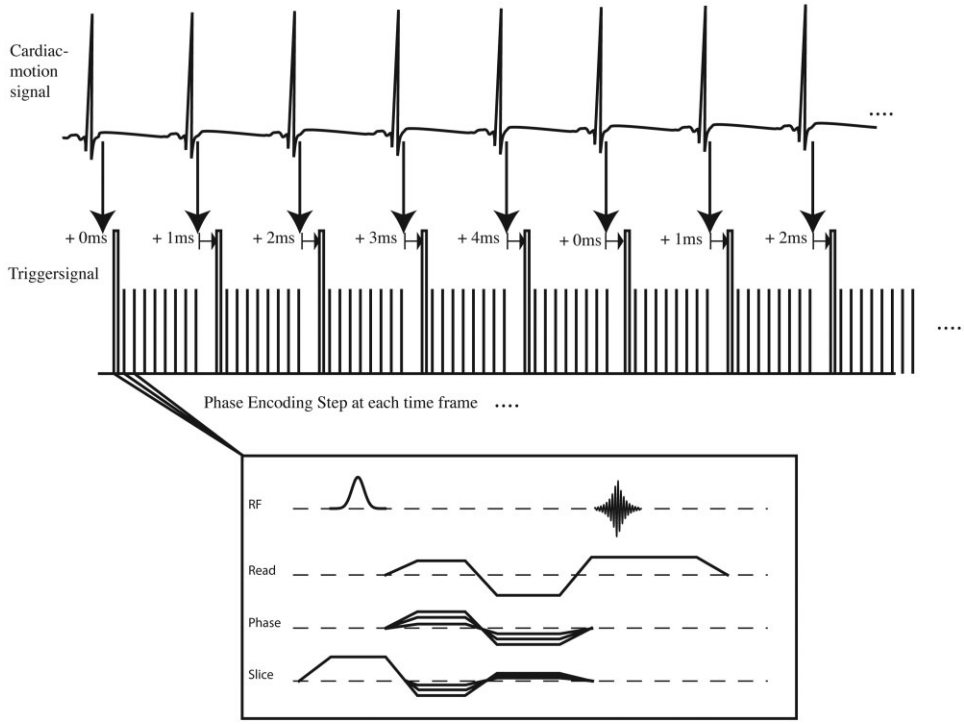

FIG. 2. Pulse-sequence for the simultaneous measurement of blood flow velocity and the cross-sectional areas. By repeating the acquisition for each CINE data set five times with a time delay of 1 ms between subsequent data sets, an effective temporal resolution of 1000 frames/s could be achieved.

basic imaging sequence consisted of a FLASH sequence with velocity compensated gradients for all three gradient directions. To detect through-plane velocity information, two additional flow encoded data sets were acquired by applying bipolar flow encoding gradients in the slice encoding direction. The first gradient moments were chosen to be (−0.3,0,0.3) s/m corresponding to a flow encoding window of 1.7 m/s.

To process flow encoded image data according to the QA-approach, a high temporal resolution is necessary to sample the systolic upstrokes of the Q- and A-curves with a sufficiently high number of data points. Therefore an interleaved acquisition scheme was implemented when applying the different phase encoding steps as shown in Fig. 2. By using a repetition time of TR = 5 ms, a total number of five similar time-delayed imaging experiments was necessary to gain a temporal resolution of 1 ms. The total measurement time for one location in the aorta was approximately 5 min. Because the calculation of the PWV requires only processing of early systolic MR data, a time window of 40 ms was sufficient. Further imaging parameters were as follows: matrix size, 160 × 160; field of view = 2.2 cm × 2.2 cm; echo time (TE) = 1.7 ms; slice thickness = 1 mm; total number of time frames = 40.

Data Processing/ Imaging

Data processing was performed using MATLAB (The Mathworks, Inc., Natick, MA). For morphometric analysis of the vessel, geometry magnitude images were imported into AMIRA (Mercury Computer Systems, Chelmsford, MA). The cross-sectional area of the vessel was segmented manually in each time frame. To reduce the standard error when outlining cross-sectional areas, all segmentations were repeated four times by the same observer. The mean area was also calculated for further computations.

Velocity information for each pixel inside the vessel was computed by fitting a line to the phase data as a function of the first moments of the velocity encoding gradients. Because three different encoding steps were applied, the quality of the linear fit gave an estimate for the error of the velocity information. Therefore, to reduce the total error of the velocity calculation, all data points with $R^2 < 0.85$ (R: correlation coefficient) were excluded from further calculations. Blood volume flow was calculated by spatially integrating all intraluminal velocity data and multiplying it by the corresponding cross-sectional areas. PWV was computed by fitting a line to those data points of the QA-plot corresponding to the early systolic pulse-wave. The start of the systolic flow pulse was determined as the point of intersection of the linear extrapolation of the early systolic slope and the flow baseline at the end diastole. To reduce random high frequency changes of the volume flow- and area-curves, a low-pass filter was applied to the data. Differences between mean values of the group samples were verified by using a two-tailed t-test. Statistical significance was assigned to *P* values less than 0.01.

RESULTS

Representative images of the ascending and the abdominal aorta can be seen in Figure 1b,c. With a temporal distance of 1 ms between two subsequent time frames, the upstroke of the systolic volume flow could be sampled with 6–10 data points. The intraluminal velocity distribution of the through-plane blood flow shows significant differences between the measurements at the ascending aorta (Fig. 3b,c) and the abdominal aorta (Fig. 3a,d). Whereas the aortic

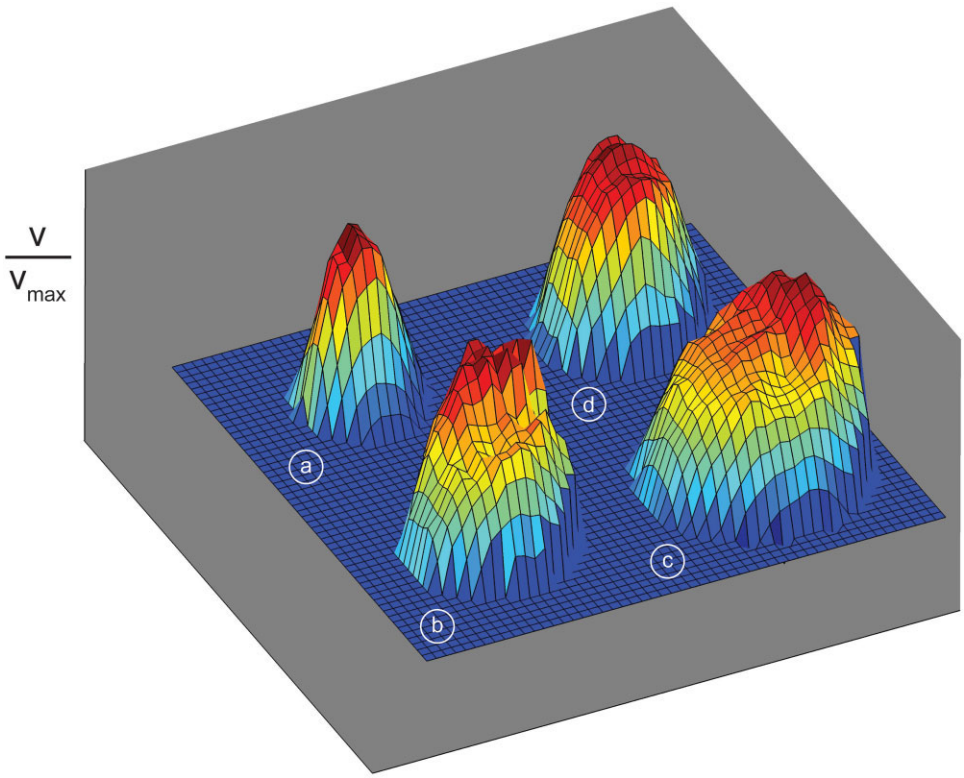

FIG. 3. Intraluminal velocity distribution for a systolic time frame in the ascending and abdominal aorta. **a:** Abdominal aorta of a C57BL/6J mouse (2 months). **b:** Ascending aorta of a C57BL/6J mouse (2 months). **c:** Ascending aorta of an apoE-KO mouse (8 months). **d:** Abdominal aorta of an apoE-KO mouse (8 months).

flow at an abdominal location represents an almost parabolic flow profile, as expected for a laminar tube flow, the results of the ascending aorta differ significantly from an ideal parabolic profile. The skewed flow patterns were observable in almost every animal in each group (apoE-KO and C57BL/6J mice) and correspond to previously published data by Feintuch et al. (31). Cross-sectional area changes of the abdominal aorta in a C57BL/6J mouse are plotted in Figure 4b. The corresponding plot of the blood volume flow is depicted in Figure 4a. A total of 40 time frames was sufficient to cover the late diastolic and the early systolic cardiac phase. When plotting cross-sectional areas versus flow-data, the experimental data was consistent with the hypothesized linear relationship for early systolic time frames (Fig. 4c). Pulse-wave velocity values ranged from 2.4 m/s (minimum C57BL/6J group, 2 months) to 4.3 m/s (maximum apoE-KO group). For the wild-type (WT) group, average PWV values measured in the ascending aorta were 2.8 ± 0.2 m/s (mean ± SE) and 2.6 ± 0.1 m/s at the age of 2 months and 8 months respectively. For the apoE-KO group, the measured PWV in the ascending aorta was 3.6 ± 0.2 m/s.

Measurements in the abdominal aorta showed similar results with PWV at 2.9 ± 0.1 m/s and 2.6 ± 0.2 m/s for the WT group (2 months and 8 months respectively) and 4.0 ± 0.2 m/s for the apoE-KO animals. Mean abdominal- and ascending-aortic-PWV in the apoE-KO group differed significantly from the results for the WT groups as shown in Table 1. PWV measurements for the WT animals at the different ages of 2 months and 8 months did not show statistically significant differences of the mean values. In addition, due to the differences in age, diet and genotype within both groups, the apoE-KO mice showed significantly higher cross-sectional areas and body weights than the 2-month-old WT group.

DISCUSSION AND CONCLUSION

The present work has shown that high field in vivo MRI has the capability to measure local PWV at different locations in the murine aorta.

Average values for the PWV of apoE-KO mice lie within the range of values of ultrasonic measurements reported in previous studies with apoE-KO-mice at the age of 13 months (3.8 ± 0.2 m/s (mean ± SE)) (32). Wang et. al reported an increase of aortic stiffness in apoE-KO mice at the age of 13 months compared with age-matched wild type controls (33). In the present study, we already observe a significant difference between 8-month-old C57BL/6J mice and age-matched apoE-KO mice. The reason for the early changes of elastic properties in the vascular wall might be the high cholesterol diet, which is supposed to accelerate aortic wall remodeling, thus increasingly leading to elastic destruction (34). The magnitude data of the complex CINE data sets gave evidence for arterial wall thickening caused by atherosclerotic lesions (Fig. 5a). Histological studies could confirm the findings of the MR measurements. A close agreement was observed between H&E-stained histopathological sections and the corresponding MR images which can be seen in Fig. 5b.

Changes of the elastic properties within the WT group due to age-related effects could not be observed. PWV values of both WT groups are similar to values obtained in 8-month-old B6D2F1 mice ([2.86 ± 0.14] m/s) with an ultrasound TT method (4). Reddy et al. have shown that arterial stiffening occurs with age by examining the PWV

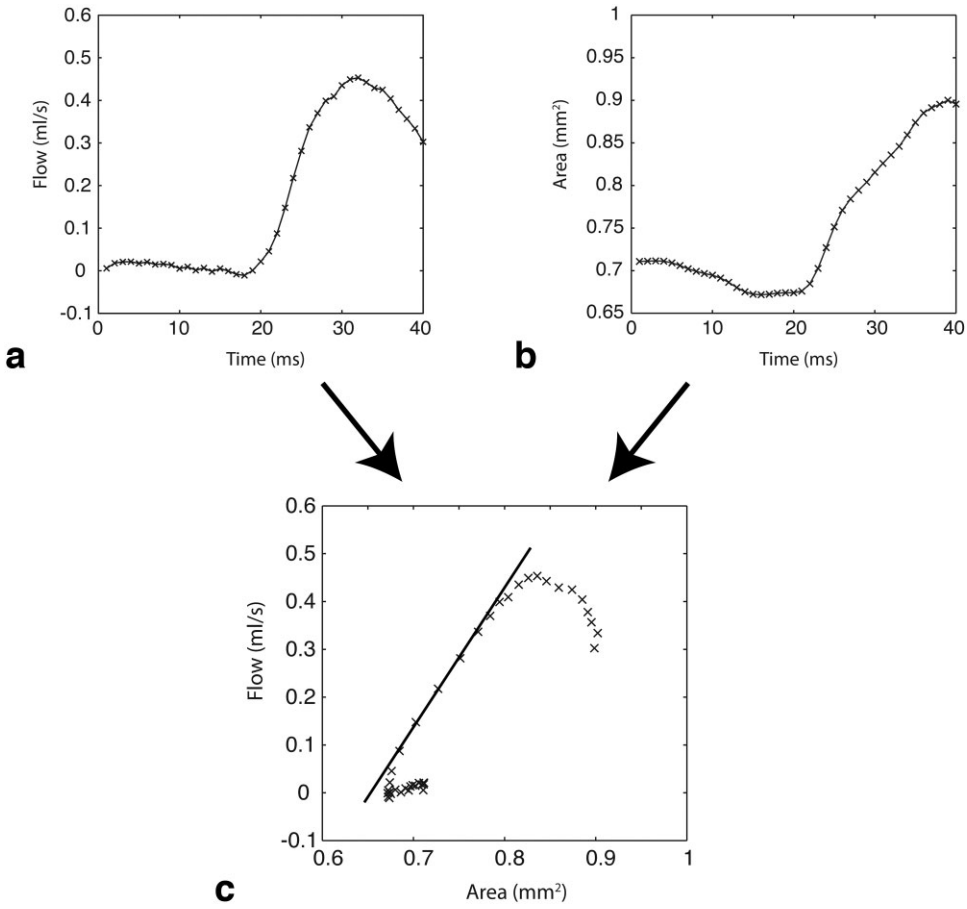

FIG. 4. Representative results of the flow–area measurements for the abdominal aorta (C57BL/6J mouse). **a:** Volume flow during late diastole and early systole. **b:** Corresponding cross-sectional area measurements. **c:** PWV determined as the slope of the flow–area relation during early systole.

and input impedance in 29-month-old B6D2F1 mice compared with an 8-month-old group (4). In the present study, no changes of the PWV could be found for the two different WT groups. In C57BL/6J mice, age-related arterial wall stiffening possibly occurs considerably later than at the age of 8 months.

A crucial parameter to all systems monitoring velocity-pulse-wave propagation in mice is the high frame rate necessary for PWV evaluation. The pure CINE imaging method did not allow for a sufficiently high temporal sample scheme. With the interleaved acquisition scheme we were able to monitor flow variations at 1000 frames/s. By applying several time-delayed CINE imaging sequences, however, the total measurement time was extended to 5 min. For this reason, the measurements were very sensitive to changes of the heart rate. During the MR experiments, the averaged deviations of the mean RR-interval ranged from 0.5 ms to 1.5 ms. Variations of the mean heart rate of more than 5 ms during the whole experiment did not allow for a reliable PWV calculation.

Compared with ultrasonic measurement, high resolution MRI methods benefit from an improved image quality, allowing for a more accurate determination of cross-sectional areas (28). The improved SNR in high-field MRI and

Table 1
Results of the Local PWV Measurements in the Ascending and the Abdominal Aorta*

Parameters	ApoE-KO	WT (2 mo)	WT (8 mo)
Weight (g)	38 ± 2	22.6 ± 0.6	30.4 ± 0.5
Ascending aorta			
Peak CSA (mm^2)	3.1 ± 0.3	*1.51 ± 0.03	2.5 ± 0.1
Peak volume flow (cm^3/s)	1.3 ± 0.2	1.13 ± 0.04	1.04 ± 0.04
PWV (m/s)	*3.6 ± 0.2	2.8 ± 0.2	2.6 ± 0.1
Abdominal aorta			
Peak CSA (mm^2)	1.52 ± 0.05	0.98 ± 0.07	1.2 ± 0.2
Peak volume flow (cm^3/s)	0.61 ± 0.06	0.48 ± 0.02	0.5 ± 0.1
PWV (m/s)	*4.0 ± 0.2	2.9 ± 0.1	2.6 ± 0.2

Data are presented as mean ± SE. Asterisks in the body of the table indicate a statistically significant difference of the mean values when compared with the WT group (8 months) ($P < 0.01$).
PWV = pulse-wave velocity; KO = knockout; WT = wild-type; CSA = cross-sectional area.

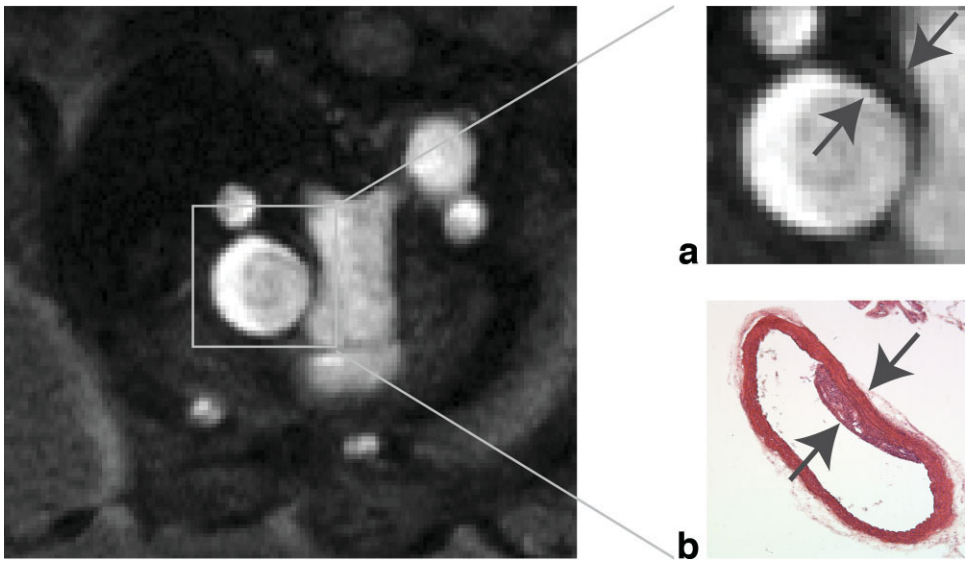

FIG. 5. **a:** Representative magnitude image of a CINE data set of an apoE-KO mouse. The arrows indicate the region of the atherosclerotic lesion in the ascending aorta. **b:** Corresponding histopathological section stained with hematoxylin and eosin.

the small size of the RF-coil allowed high resolution acquisitions without averaging. For this reason, when examining the local PWV, sufficient SNR becomes a crucial point because the total measurement time must be minimized to ensure a stable heart rate during the entire experiment. Because the area changes are only a few pixels between two consecutive time frames, it was necessary to repeat image segmentation several times to calculate mean values and minimize error. Moreover the signal enhancement of nonsaturated fast inflowing blood possibly leads to an underestimation of the aortic cross-section, because pixel of almost-static tissue, such as the vessel wall and outer regions of the vessel, carry comparatively poor signal intensity.

The major assumption to apply the QA-method is a reflection-free pulse-wave. The nonuniform geometry and elasticity of the arterial system leads to wave reflection sites all over the arterial tree. In humans, the principal reflection sites are supposed to be the microvascular beds (25). The arterioles are recognized to cause the principal change of the vascular impedance leading to wave reflections. Thus, the QA-method should be applied sufficiently upstream from changes of vascular impedance. The time interval between the initial pulse and the principal reflected pulse-wave is considerably higher at the ascending aorta than at the abdominal aorta. In this respect the ascending aorta would be the most appropriate arterial vessel for applying the QA-method. Assuming pulse-wave velocities, however, in the range of 3 to 5 m/s, the reflected pulse-wave would take approximately 5–10 ms to return to the abdominal aorta, still allowing for a sufficient high number of data points when imaging at 1000 fps.

A major drawback with the assessment of the PWV in the ascending aorta is the nonparabolic skewed flow pattern observed during early systole. Velocity profiles similar to that of Dean vortices lead to nonreproducible phase values for certain intraluminal voxels (31,35,36). Because three flow encoding steps were acquired, possible errors in the calculation of the volume flow could be reduced by excluding velocity information from pixels with R^2 being less than 0.85.

Segmentation of cross-sectional areas during early systole sometimes suffers from signal loss due to high blood flow rates. Spatial misalignment effects occur especially when imaging the aortic arch, because the vessel runs perpendicular to the imaging slice only for approximately 2–3 mm. The completely flow compensated design of the MR sequence and the short TE allowed a significant reduction of flow artifacts, thus avoiding resultant errors in the segmentation. The short TE also resulted in a reduction of susceptibility artifacts, which are one of the main sources of reduced image quality in measurements at 17.6T. Artifacts caused by local field inhomogeneities, however, did not allow the investigation of vessels close to lung tissue.

According to previously published work on the errors in PC-MRI volumetric flow measurements, the error for flux calculation in the current work can be estimated (37). Assuming an inner vessel diameter of 1 mm, the relative error due to partial volume effects does not exceed 3%. The error due to a misalignment angle of less than 15° between the flow-encoding axes and the blood flow direction is below 5%. Partial volume effects close to the vessel wall also cause an error in cross-sectional area segmentation. In the case of parabolic flow profiles with zero blood flow at the vessel wall, the areal error is significantly higher than the errors of the flux calculation. Repeated cross-sectional area segmentation reduced the relative standard error of the planimetry to 2.2%.

This study demonstrates the feasibility of high field MRI to estimate local PWV at different sites in the murine aorta. The pulse-wave velocities determined with the presented QA-method correspond to reported data and allow for a distinction between mean values of different groups. Compared with similar approaches in humans, the simultaneous acquisition of area- and flow-information could reduce the total acquisition time, a crucial point in terms of maintaining a constant heart rate. Because MRI has already shown its capabilities in investigating vessel wall morphology in mice, the presented method could add the accessibility of a further functional parameter. Due to the short total measurement time of only a few minutes, a combination of vessel wall visualization experiments and

functional examinations by PWV-measurements would allow for a comprehensive set of parameters characterizing the vascular system.

ACKNOWLEDGMENTS

This study was supported by the Deutsche Forschungsgemeinschaft in the scope of Sonderforschungsbereich 688. We thank Ashley and Thomas Basse-Lüsebrink for valuable comments on the manuscript.

REFERENCES

1. Arnett DK, Evans GW, Riley WA. Arterial stiffness: a new cardiovascular risk factor? Am J Epidemiol 1994;140:669–682.
2. Laurent S, Katsahian S, Fassot C, Tropeano AI, Gautier I, Laloux B, Boutouyrie P. Aortic stiffness is an independent predictor of fatal stroke in essential hypertension. Stroke 2003;34:1203–1206.
3. Lang RM, Cholley BP, Korcarz C, Marcus RH, Shroff SG. Measurement of regional elastic properties of the human aorta. A new application of transesophageal echocardiography with automated border detection and calibrated subclavian pulse tracings. Circulation 1994;90:1875–1882.
4. Reddy AK, Li YH, Pham TT, Ochoa LN, Trevino MT, Hartley CJ, Michael LH, Entman ML, Taffet GE. Measurement of aortic input impedance in mice: effects of age on aortic stiffness. Am J Physiol Heart Circ Physiol 2003;285:H1464–H1470.
5. Blacher J, Guerin AP, Pannier B, Marchais SJ, Safar ME, London GM. Impact of aortic stiffness on survival in end-stage renal disease. Circulation 1999;99:2434–2439.
6. Blacher J, Pannier B, Guerin AP, Marchais SJ, Safar ME, London GM. Carotid arterial stiffness as a predictor of cardiovascular and all-cause mortality in end-stage renal disease. Hypertension 1998;32:570–574.
7. Reddick RL, Zhang SH, Maeda N. Atherosclerosis in mice lacking apo E. Evaluation of lesional development and progression. Arterioscler Thromb 1994;14:141–147.
8. Nakashima Y, Plump AS, Raines EW, Breslow JL, Ross R. ApoE-deficient mice develop lesions of all phases of atherosclerosis throughout the arterial tree. Arterioscler Thromb 1994;14:133–140.
9. Osada J, Joven J, Maeda N. The value of apolipoprotein E knockout mice for studying the effects of dietary fat and cholesterol on atherogenesis. Curr Opin Lipidol 2000;11:25–29.
10. Neuberger T, Greiser A, Nahrendorf M, Jakob PM, Faber C, Webb AG. 23Na microscopy of the mouse heart in vivo using density-weighted chemical shift imaging. MAGMA 2004;17:196–200.
11. Nahrendorf M, Streif JU, Hiller K-H, Hu K, Nordbeck P, Ritter O, Sosnovik D, Bauer L, Neubauer S, Jakob PM, Ertl G, Spindler M, Bauer WR. Multimodal functional cardiac MRI in creatine kinase-deficient mice reveals subtle abnormalities in myocardial perfusion and mechanics. Am J Physiol Heart Circ Physiol 2006;290:H2516–H2521.
12. Choudhury RP, Fayad ZA, Aguinaldo JG, Itskovich VV, Rong JX, Fallon JT, Fisher EA. Serial, noninvasive, in vivo magnetic resonance microscopy detects the development of atherosclerosis in apolipoprotein E-deficient mice and its progression by arterial wall remodeling. J Magn Reson Imaging 2003;17:184–189.
13. Fayad ZA, Fallon JT, Shinnar M, Wehrli S, Dansky HM, Poon M, Badimon JJ, Charlton SA, Fisher EA, Breslow JL, Fuster V. Noninvasive in vivo high-resolution magnetic resonance imaging of atherosclerotic lesions in genetically engineered mice. Circulation 1998;98:1541–1547.
14. Hockings PD, Roberts T, Galloway GJ, Reid DG, Harris DA, Vidgeon-Hart M, Groot PH, Suckling KE, Benson GM. Repeated three-dimensional magnetic resonance imaging of atherosclerosis development in innominate arteries of low-density lipoprotein receptor-knockout mice. Circulation 2002;106:1716–1721.
15. Itskovich VV, Choudhury RP, Aguinaldo JG, Fallon JT, Omerhodzic S, Fisher EA, Fayad ZA. Characterization of aortic root atherosclerosis in ApoE knockout mice: high-resolution in vivo and ex vivo MRM with histological correlation. Magn Reson Med 2003;49:381–385.
16. Schneider JE, McAteer MA, Tyler DJ, Clarke K, Channon KM, Choudhury RP, Neubauer S. High-resolution, multicontrast three-dimensional-MRI characterizes atherosclerotic plaque composition in ApoE-/- mice ex vivo. J Magn Reson Imaging 2004;20:981–989.
17. Wiesmann F, Szimtenings M, Frydrychowicz A, Illinger R, Hunecke A, Rommel E, Neubauer S, Haase A. High-resolution MRI with cardiac and respiratory gating allows for accurate in vivo atherosclerotic plaque visualization in the murine aortic arch. Magn Reson Med 2003;50:69–74.
18. Macgowan CK, Henkelman RM, Wood ML. Pulse-wave velocity measured in one heartbeat using MR tagging. Magn Reson Med 2002;48:115–121.
19. Rogers WJ, Hu YL, Coast D, Vido DA, Kramer CM, Pyeritz RE, Reichek N. Age-associated changes in regional aortic pulse wave velocity. J Am Coll Cardiol 2001;38:1123–1129.
20. Vulliémoz S, Stergiopulos N, Meuli R. Estimation of local aortic elastic properties with MRI. Magn Reson Med 2002;47:649–654.
21. Yu H-Y, Peng H-H, Wang J-L, Wen C-Y, Tseng W-YI. Quantification of the pulse wave velocity of the descending aorta using axial velocity profiles from phase-contrast magnetic resonance imaging. Magn Reson Med 2006;56:876–883.
22. Hartley CJ, Reddy AK, Madala S, Entman ML, Michael LH, Taffet GE. Noninvasive ultrasonic measurement of arterial wall motion in mice. Am J Physiol Heart Circ Physiol 2004;287:H1426–H1432.
23. Hartley CJ, Reddy AK, Madala S, Martin-McNulty B, Vergona R, Sullivan ME, Halks-Miller M, Taffet GE, Michael LH, Entman ML, Wang YX. Hemodynamic changes in apolipoprotein E-knockout mice. Am J Physiol Heart Circ Physiol 2000;279:H2326–H2334.
24. Hartley CJ, Taffet GE, Michael LH, Pham TT, Entman ML. Noninvasive determination of pulse-wave velocity in mice. Am J Physiol 1997;273:H494–H500.
25. Li JKJ. Dynamics of the vascular system. River Edge, NJ: World Scientific; 2004.
26. Rabben SI, Stergiopulos N, Hellevik LR, Smiseth OA, Slørdahl S, Urheim S, Angelsen B. An ultrasound-based method for determining pulse wave velocity in superficial arteries. J Biomech 2004;37:1615–1622.
27. Vulliémoz S, Stergiopulos N, Meuli R. Estimation of local aortic elastic properties with MRI. Magn Reson Med 2002;47:649–654.
28. Williams R, Needles A, Cherin E, Zhou YQ, Henkelman RM, Adamson SL, Foster FS. Noninvasive ultrasonic measurement of regional and local pulse-wave velocity in mice. Ultrasound Med Biol 2007;33:1368–1375.
29. Markl M, Dudler P, Fydrychowicz A, Strecker C, Weiller C, Hennig J, Harloff A. Optimized 3D bright blood MRI of aortic plaque at 3 T. Magn Reson Imaging 2008;26:330–336.
30. Markl M, Draney MT, Miller DC, Levin JM, Williamson EE, Pelc NJ, Liang DH, Herfkens RJ. Time-resolved three-dimensional magnetic resonance velocity mapping of aortic flow in healthy volunteers and patients after valve-sparing aortic root replacement. J Thorac Cardiovasc Surg 2005;130:456–463.
31. Feintuch A, Ruengsakulrach P, Lin A, Zhang J, Zhou YQ, Bishop J, Davidson L, Courtman D, Foster FS, Steinman DA, Henkelman RM, Ethier CR. Hemodynamics in the mouse aortic arch as assessed by MRI, ultrasound, and numerical modeling. Am J Physiol Heart Circ Physiol 2007;292:H884–H892.
32. Wang YX, Halks-Miller M, Vergona R, Sullivan ME, Fitch R, Mallari C, Martin-McNulty B, da Cunha V, Freay A, Rubanyi GM, Kauser K. Increased aortic stiffness assessed by pulse wave velocity in apolipoprotein E-deficient mice. Am J Physiol Heart Circ Physiol 2000;278:H428–H434.
33. Wang Y-X. Cardiovascular functional phenotypes and pharmacological responses in apolipoprotein E deficient mice. Neurobiol Aging 2005;26:309–316.
34. Zhang SH, Reddick RL, Burkey B, Maeda N. Diet-induced atherosclerosis in mice heterozygous and homozygous for apolipoprotein E gene disruption. J Clin Invest 1994;94:937–945.
35. Dean WR. Note on the motion of fluid in a curved pipe. Philos Mag 1927;4:208–223.
36. Dean WR. The stream line motion of fluid in a curved pipe. Philos Mag 1928;5:674–695.
37. Wolf RL, Ehman RL, Riederer SJ, Rossman PJ. Analysis of systematic and random error in MR volumetric flow measurements. Magn Reson Med 1993;30:82–91.